Rare earth element diffusion in diopside: Influence of temperature, pressure, and ionic radius, and an elastic model fordiffusion in silicates

Article *in* Contributions to Mineralogy and Petrology · September 2001

DOI: 10.1007/s004100100269

CITATIONS
334

READS
275

3 authors:

James A Van Orman
Case Western Reserve University
175 PUBLICATIONS **3,841** CITATIONS

SEE PROFILE

Timothy L Grove
Massachusetts Institute of Technology
420 PUBLICATIONS **22,741** CITATIONS

SEE PROFILE

Nobumichi Shimizu
Woods Hole Oceanographic Institution
133 PUBLICATIONS **7,939** CITATIONS

SEE PROFILE

Contrib Mineral Petrol (2001) 141: 687–703
DOI 10.1007/s004100100269

James A. Van Orman · Timothy L. Grove
Nobumichi Shimizu

Rare earth element diffusion in diopside: influence of temperature, pressure, and ionic radius, and an elastic model for diffusion in silicates

Received: 20 December 2000 / Accepted: 23 March 2001 / Published online: 14 July 2001

Abstract Volume diffusion rates for five rare earth elements (La, Ce, Nd, Dy, and Yb) have been measured in single crystals of natural diopside at pressures of 0.1 MPa to 2.5 GPa and temperatures of 1,050 to 1,450 °C. Polished, pre-annealed crystals were coated with a thin film of rare earth element oxides, then held at constant temperature and pressure for times ranging from 20 to 882 h. Diffusion profiles in quenched samples were measured by SIMS (secondary ion mass spectrometry) depth profiling. At 1 atm pressure, with the oxygen fugacity controlled near the quartz–fayalite–magnetite buffer, the following Arrhenius relations were obtained for diffusion normal to (001) (diffusion coefficient D in m^2/s): $\log_{10}D_{Yb} = (-4.64 \pm 0.42) - (411 \pm 12$ kJ/mol/$2.303RT$); $\log_{10}D_{Dy} = (-3.31 \pm 1.44) - (461 \pm 41$ kJ/mol/$2.303RT$); $\log_{10}D_{Nd} = (-2.95 \pm 2.64) - (496 \pm 77$ kJ/mol/$2.303RT$); $\log_{10}D_{Ce} = (-4.10 \pm 1.08) - (463 \pm 31$ kJ/mol/$2.303RT$); $\log_{10}D_{Lu} = (-4.22 \pm 2.66) - (466 \pm 78$ J/mol/$2.303RT$).

Diffusion rates decrease significantly with increasing ionic radius, with La a factor of ~35 slower than Yb. The relationship between diffusivity and ionic radius is consistent with a model in which elastic strain plays a critical role in governing the motion of an ion through the crystal lattice. Activation volumes for Yb and Ce diffusion, at constant temperature and oxygen fugacity, are 9.0 ± 2.0 cm^3/mol and 8.9 ± 3.2 cm^3/mol, respectively, corresponding to an order of magnitude decrease in diffusivity as pressure is increased from 0 to 3 GPa at 1,200 °C. Diffusion of Nd is such that grain-scale isotopic equilibrium in the mantle can be achieved in ~1 My under conditions near the peridotite solidus (~1,450 °C at 2.5 GPa). The equilibration time is much longer under P, T conditions of the lithospheric mantle or at the eclogite solidus (~1 Gy at 1.5 GPa and 1,150 °C). Because of the relatively strong decrease in diffusivity with pressure (two orders of magnitude between 2.5 and 15 GPa along an adiabatic temperature gradient), Nd transport in clinopyroxene will be effectively frozen at pressures approaching the transition zone, on time scales less than 100 My. Rare earth element diffusion rates are slow enough that significant disequilibrium uptake of REE by growing clinopyroxene phenocrysts may be preserved under natural conditions of basalt crystallization. The relative abundances and spatial distributions of REE in such crystals may provide a sensitive record of the cooling and crystallization history of the host lava.

J.A. Van Orman (✉) · T.L. Grove
Department of Earth, Atmospheric, and Planetary Sciences,
Massachusetts Institute of Technology,
Cambridge, MA 02139, USA

N. Shimizu
Department of Geology and Geophysics,
Woods Hole Oceanographic Institution,
Woods Hole, MA 02543, USA

Present address: J.A. Van Orman
Carnegie Institution of Washington,
Geophysical Laboratory and Department of
Terrestrial Magnetism, 5251 Broad Branch Rd,
N.W., Washington, DC 20015, USA
e-mail: j.van_orman@gl.ciw.edu

Editorial responsibility: J. Hoefs

Introduction

High-Ca pyroxene is an important host for rare earth elements in the Earth's mantle, and its diffusion properties have a central role in determining the spatial and temporal scales of REE transport. Diffusion in high-Ca pyroxene may control the redistribution of REE and other trace elements during the production and transport of melt (e.g., Qin 1992; Hart 1993; Iwamori 1993; Van Orman et al. 1998), during solid-state phase transformations (e.g., Koga et al. 1999), and during phenocryst growth from basaltic magmas (e.g., Albarède and Bottinga 1972; Shimizu 1981; Watson and Liang 1995; Watson 1996). Information on the time scales of these processes can be obtained provided that the appropriate diffusion coefficients are known.

This paper presents experiments on rare earth element diffusion rates in diopside, a representative high-Ca pyroxene with the chemical formula $CaMgSi_2O_6$. The influence of temperature, pressure, and oxygen fugacity on REE diffusivity are examined at pressures up to 2.5 GPa, over a temperature range that spans the peridotite solidus. Although the rare earth elements share similar properties, small differences in ionic radii can lead to pronounced differences in geochemical behavior. One example is the strong preferential partitioning of heavy REE relative to light REE into high-Ca pyroxene. Differences in ionic radius may similarly affect diffusion rates, with the potential to induce diffusive fractionation of the rare earth elements. We have determined diffusion coefficients for five rare earth elements, La, Ce, Nd, Dy, and Yb, with ionic radii between 0.099 and 0.116 nm. The data show a systematic decrease in diffusivity with increasing ionic radius, and this trend is shown to be consistent with a model in which a large fraction of the migration energy is expended in elastic strain of the crystal lattice. The diffusion rates we report are significantly slower than a previous determination of Sm diffusivity in diopside (Sneeringer et al. 1984). The present data suggest that long-held views on the length scales of chemical and isotopic heterogeneity in Earth's mantle (e.g., Hofmann and Hart 1978) need to be reconsidered.

Experimental methods

Diffusion coefficients were determined from isothermal annealing experiments in which an oriented, polished diopside single crystal was coated with a thin layer of REE oxides and then held at constant temperature and pressure for a certain period of time, ranging between 20 and 882 h. Diffusion profiles in quenched samples were measured by SIMS (secondary ion mass spectrometry) depth profiling, and diffusion coefficients were determined by fitting the profiles to an appropriate solution of the diffusion equation. Most experiments were designed to examine diffusion of two or three rare earth elements in the same experiment. This approach reduced the uncertainty in the relative diffusion rates of the elements, and was more efficient than performing a separate set of experiments for each element. In order to determine whether multicomponent coupling effects among the REE may have been important in these experiments (in other words, whether the concentration gradient in one element may have influenced the diffusive flux of another), a subset of diffusion experiments was performed in which Ce oxide alone was deposited in the tracer layer.

The influence of temperature on diffusion of the rare earth elements was evaluated by performing a set of experiments at atmospheric pressure between 1,050 and 1,300 °C. The oxygen fugacity in these experiments was controlled near the quartz–fayalite–magnetite (QFM) buffer, similar to the f_{O_2} inferred for mid-ocean ridge basalts (Christie et al. 1986). One experiment was also performed with the oxygen fugacity held four $\log_{10}$ units above the QFM buffer, as a preliminary investigation of the influence of f_{O_2} on REE diffusivity. A set of piston-cylinder experiments was performed to evaluate the influence of pressure on diffusion of Ce and Yb, at pressures of 1.3 to 2.5 GPa and temperatures of 1,250 to 1,450 °C.

In the present study we have focused on diffusion normal to the (001) plane. Previous studies of Sr, Ca, and Pb diffusion in diopside (Sneeringer et al. 1984; Dimanov et al. 1996; Cherniak 1998a; Dimanov and Jaoul 1998) have found no evidence of significant anisotropy, and we tentatively expect that the REE, which partition onto the same crystallographic site (M2), behave similarly in this respect.

Starting material

The starting material for the diffusion experiments consisted of gem-quality diopside single crystals from the Kunlun Mountains, China. These crystals are from the same locality as those used by Van Orman et al. (1998) in a study of U and Th diffusion in diopside. The crystals were free of cracks and visible inclusions and homogeneous in major element composition, as determined by electron microprobe (Table 1). Well-developed {100}, {010}, {001}, {110}, and {111} growth faces were present, and these allowed the crystals to be oriented visually with respect to their crystallographic axes. Each crystal was cut perpendicular to (001) into wafers ~0.5 mm thick. One side of each wafer was mechanically polished with diamond and alumina pastes, then chemically polished with an alkaline colloidal silica (0.06 μm) suspension. The polished diopside wafers were rinsed in purified water, then pre-annealed for 1 to 2 days at 1,150–1,200 °C under a controlled atmosphere. The purpose of this pre-annealing step is to heal surface damage caused by polishing and to equilibrate point defects under temperature and f_{O_2} conditions near those to be used in the diffusion experiments.

1 atm diffusion anneals

The tracer layer was deposited by evaporating an aqueous solution onto the polished, pre-annealed surface of the diopside. Four different tracer solutions were used, containing Ce, Ce + Yb, La + Nd + Dy, and Yb, respectively, each in dilute (~0.05 M) nitric acid with ~300–500 ppm REE. The solutions were mixed in 1:1 proportions with methanol, which acted as a surfactant, and a few drops (~10 μl) were delivered to the polished diopside surface with a microsyringe. After allowing the solution to evaporate on a hot plate at 120 °C, the nitrates were decomposed by heating the sample in a furnace for 10 min at 800 °C, leaving a thin layer of REE oxides on the surface. This thin oxide layer, consisting of microcrystalline particles, provided the tracer source for the diffusion experiments. We did not analyze the surface coating by X-ray diffraction, but optical examination confirmed that the layer was crystalline. We did not check whether any nitrates remained on the surface after the initial heating, but because REE nitrates decompose at very low temperatures, we do not expect them to have been present unless they immediately reacted with the diopside surface. Optical examination revealed no evidence for such a reaction either before or after the diffusion anneal. The total concentration of REE in the tracer layer was approximately 0.2 $\mu g/mm^2$.

Samples were placed in open Pt crucibles with the coated side facing up and held in the hotspot of a Deltech DT31VT vertical gas mixing furnace for times ranging from 23 to 882 h. The tempera-

Table 1 Kunlun Mountains diopside composition. Weight % is average of 15 electron microprobe analyses of three different crystals. Numbers in parentheses represent one standard deviation

Oxide	Weight %
SiO_2	55.75 (0.34)
TiO_2	0.04 (0.01)
Al_2O_3	0.88 (0.17)
Cr_2O_3	0.02 (0.01)
FeO*	0.70 (0.07)
MnO	0.05 (0.02)
MgO	17.73 (0.36)
CaO	24.53 (0.29)
Na_2O	0.48 (0.09)
Total	100.2 (0.6)

ture and oxygen fugacity were adjusted to run conditions before introducing the sample into the furnace, and were held constant during the diffusion anneal. Temperature was monitored continuously with a $Pt–Pt_{90}Rh_{10}$ thermocouple calibrated against the melting points of NaCl, Au, and Pd on the IPTS 1968 temperature scale, and fluctuated within less than 2 °C over the course of each experiment. Oxygen fugacity was controlled by mixing CO_2 and H_2 gases and was monitored using a solid ZrO_2–CaO electrolyte oxygen sensor calibrated against the Fe–FeO, Ni–NiO, and $Cu–Cu_2O$ buffers. Variation in f_{O_2} during an experiment was within less than 0.1 log unit. Samples were quenched by removing the Pt bucket from the furnace and allowing it to cool in air.

After the diffusion anneal, the diopside crystals were rinsed ultrasonically in purified H_2O and examined with reflected light and scanning electron microscopes. Recrystallization and surface migration took place within the tracer layer during the diffusion anneal, as evidenced by the formation of coarser REE oxide crystals and more isolated islands of coating compared to the starting samples. The surface of each diopside wafer maintained a mirror finish at the end of the anneal, and there was no optical evidence in any of the samples for chemical reaction with the REE oxide coating. There was no evidence for an exsolved glassy phase, as has been observed by several authors (e.g., Ingrin et al. 1991; Doukhan et al. 1993; Dimanov et al. 1996) in Fe-bearing pyroxenes, below the nominal melting point. Glassy precipitates, if present in our samples, are too small to be observed optically.

High pressure diffusion anneals

High pressure diffusion anneals were performed in 0.5 in solid-medium piston-cylinder devices (Boyd and England 1960). A polished diopside wafer, pre-annealed under QFM buffered conditions at 1,150–1,200 °C and coated with Ce and Yb oxides using the method described above, was loaded with packed graphite powder into a cylindrical 0.175-in-diameter Pt capsule. The coated surface of the diopside was carefully positioned in the center (hotspot) of the capsule. Most of the experiments were run with the sample in direct contact with graphite powder, but two experiments were run with the sample wrapped in Pt foil within graphite powder, and one sample was placed in a sealed $Au_{80}Pd_{20}$ inner capsule that was surrounded by powdered NaCl within the Pt outer capsule. After drying for 24–48 h at 120 °C, the Pt outer capsule was welded shut, placed into a high-density alumina sleeve, and centered in a straight-walled graphite furnace using crushable MgO spacers. This assembly was then inserted into a sintered barium carbonate sleeve that served both as a thermal insulator and as a soft pressure medium. Pressure for our piston-cylinder assembly has been calibrated using the Ca-tschermakite breakdown reaction (Hays 1966). The friction correction is found to be less than 0.1 GPa at 1.3 GPa and 1,350 °C, and the pressures reported in Table 4 do not include any friction correction.

Temperature was monitored with a $W_{97}Re_3–W_{75}Re_{25}$ thermocouple that was separated from the Pt capsule by a thin crushable MgO wafer. The temperature difference between the center of the capsule and the position of the thermocouple has been determined to be 20 °C using offset thermocouples, and temperatures reported in Table 4 are corrected for this difference. No correction for the effect of pressure on thermocouple emf has been applied. Each sample was pressed cold to 0.7 GPa and then heated at 100 °C/min to 865 °C. After a 6 min hold at 865 °C and 0.7 GPa, the sample was compressed to run pressure and heated to run temperature at a rate of 50 °C/min. Experiments were held at constant temperature and pressure for times ranging from 20 to 76 h and afterward were quenched by shutting off the power. After quenching, the diopside single crystal was carefully removed from the capsule and ultrasonically rinsed in purified water. Some of the crystals were cracked in a few places, but in each sample large crack-free regions were available for analysis by SIMS depth profiling. The cracks were widely spaced compared to REE diffusion distances, and had no influence on the diffusion profiles in the regions sampled by SIMS depth profiling.

Analyses

Diffusion profiles in the annealed diopside crystals were measured using the Cameca Ims 3f ion microprobe at the Woods Hole Oceanographic Institution. Each sample was mounted in epoxy with the polished, tracer-coated surface exposed and covered with a thin (~20 nm) gold film. A primary beam of O^- ions, accelerated under a potential of 8.2 kV and with the total current held constant between 10 and 40 nA, was focused onto the sample surface to a diameter of 20–30 μm. The primary beam was rastered over a square area on a region of the diopside surface that was flat and free of large patches of REE oxides. Secondary ions produced as the primary beam sputtered through the diopside crystal were analyzed in a magnetic sector mass spectrometer. The secondary voltage was offset by –50 V, with a 20-V energy window, to reduce the contribution of molecular ions. Isotopes of the REE were monitored throughout the depth profiling analysis by repeatedly cycling through a sequence of ascending masses. ^{30}Si and ^{44}Ca were also monitored to check the stoichiometry of the analyses and to keep track of any instrumental drift. Beyond the first one or two cycles, ^{30}Si and ^{44}Ca intensities were nearly constant. The measured intensities for each mass were adjusted to the midpoint of the cycle by linear interpolation so that concentrations for each element would refer to the same depth. No standardization was used to convert secondary ion intensities to absolute concentrations; instead, diffusion coefficients were calculated directly from profiles of $REE/^{30}Si$ intensity ratios.

A circular field aperture was inserted into the secondary ion optics to restrict data collection to the flat central portion of the sputtered area and thus to minimize contamination of the diffusion profile with material from the tracer layer. In most analyses the sputtered area was 150×150 μm^2, and sampling was restricted to a central circular region 68 μm in diameter, but for some samples it was necessary to reduce the sampled area to an 8 μm circle in order to avoid coarse REE oxide crystals. Even with the field aperture, it was impossible to completely eliminate contamination from the surface tracer material during collection of the upper part of the diffusion profile. Small, heterogeneously distributed REE oxide crystals were present everywhere on the diopside surface, and these were inevitably sampled along with the diopside over the first several cycles. It was possible to identify the contaminated part of the diffusion profile, as discussed below, and these data points were not included when calculating diffusion coefficients.

Following the depth profiling analysis, the gold coat was removed by rinsing the sample in an aqueous potassium iodide solution (Ryerson and McKeegan 1994), and the depth of the sputtered pit was measured using a Sloan Dektak 8000 surface-contact profilometer equipped with a 2.5-μm diamond-tipped stylus. Several scans of each pit were made, from at least three different directions, and the mean depth over the central ~70 μm of the sputtered area was considered. The uncertainty in the depth estimate was set primarily by the roughness and curvature of the diopside surface, and was estimated to be between 20 and 40 nm in most cases. Pits that were sputtered under the same beam conditions for different times yielded consistent estimates of the sputtering rate. This confirms that the sputtering rate during a depth profiling analysis was constant, and that diffusion profiles measured as a function of sputtering time could be scaled linearly to depth.

Determination of diffusion coefficients

Diffusion in our experiments can be modeled as one-dimensional diffusion into a semi-infinite medium, with a constant concentration boundary condition at the interface between the diopside and the tracer layer. The solution to the diffusion equation under these conditions is (Crank 1975):

$$\frac{C(x,\,t) - C_0}{C_i - C_0} = erf\left(\frac{x}{2\sqrt{Dt}}\right), \tag{1}$$

where C refers to the concentration at depth x after annealing time t, C_0 is the concentration at the interface, C_i is the initial concen-

tration in the diopside crystal, and D is the diffusion coefficient. Diffusivities were evaluated by plotting the inverse error function of the left-hand side of Eq. (1) versus depth (Fig. 1a). This results in a straight line of slope $(4Dt)^{-1/2}$ if the data satisfy the conditions of the diffusion model. The erf^{-1} profiles were fitted by linear least squares regression, with the value of C_0 adjusted by an iterative procedure until the fitted line passed through the origin. Only the linear segment of the inverse error function profiles was considered in the fitting procedure. The shallow portion of most erf^{-1} profiles is steep and curved, and is considered to represent contamination from the REE oxide surface layer. Depth profiles measured on samples that were coated with REE oxides but not annealed ("zero-time" experiments) were very similar in length and in form to the near-surface segment of the profiles from annealed samples, with high surface REE intensities falling to background levels over a depth of 50–75 nm. The linear portion of the erf^{-1} profiles in most annealed samples began at a depth of 120 nm or less, and on exceptionally "clean" surfaces could be observed at a depth as shallow as 20 nm. Diffusion coefficients were determined only from diffusion profiles that extended significantly beyond the contaminated region (greater than a factor of 2) and exhibited a distinct linear segment on the inverse error function plot.

The diffusion model we have used to fit the data relies on the assumption that the REE concentrations at the interface between the tracer layer and the diopside remain constant throughout the experiment, which in turn implies that there is no resistance to ion exchange at the interface. If there is an interface resistance, then C_0 will creep upward slowly during the experiment, and the diffusion coefficients obtained by fitting the data to Eq. (1) will be in error. We emphasize that this will be the case *only* if there is an interface resistance; C_0 will remain constant, and an equation of the form of Eq. (1) will apply, even if diffusion in the tracer layer is too slow to allow REE partitioning at the interface to reach a saturation condition (Crank 1975, p. 38). A time series study at 1,200 °C revealed no evidence of a systematic variation in C_0 with increasing anneal duration, for anneal times of 119 to 456 h. There is a factor of ~2 scatter in the C_0 data at 1,200 °C, but no tendency for an increase (or decrease) in C_0 with time. This observation, combined with the excellent fits of the diffusion profiles to Eq. (1), suggests that the experiments meet the conditions of the diffusion model.

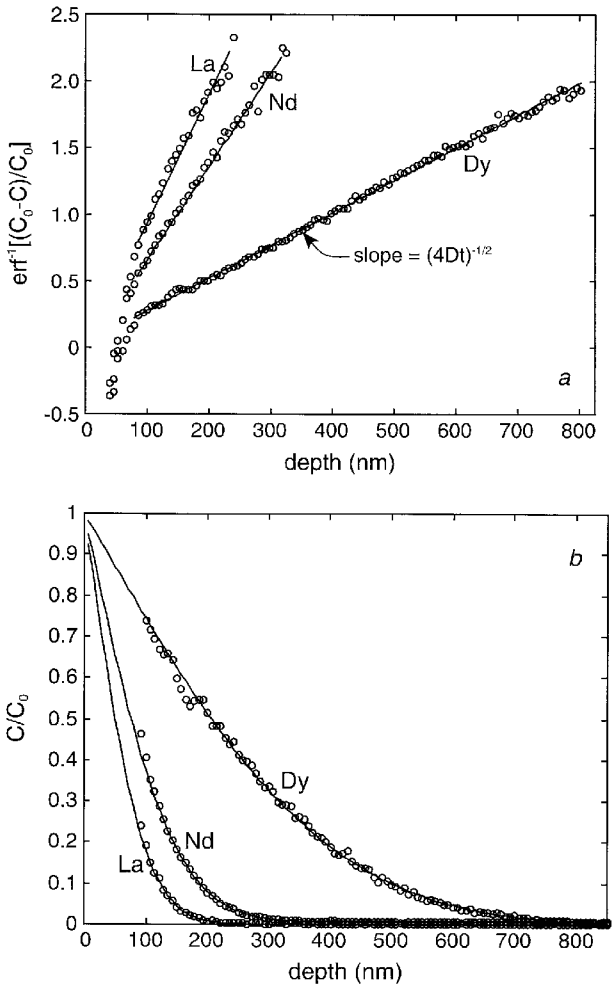

Fig. 1 Typical diffusion profiles (experiment LaNdDy2 – 1,275 °C, 0.1 MPa, 76.9 h). **a** Plot of $\text{erf}^{-1}[(C_0\text{–}C)/C_0]$ versus depth in nanometers. C represents [REE/^{30}Si] in counts per second, and C_0 is the interface concentration [adjusted in the fitting procedure so that the linear portion of each diffusion profile passes through the point (0,0)]. Profiles for La, Nd, and Dy overlap in the shallow region, but fall along distinct linear trends beyond a depth of ~90 nm. The shallow part of the profile is considered to reflect sampling of heterogeneously distributed REE oxide crystals remaining on the diopside surface after the experiment, and only the linear portion of the profile is fitted to obtain the diffusion coefficient. In **b** the concentration data are plotted versus depth, along with fitted error function curves

Results

The results of diffusion anneals performed under atmospheric pressure are listed in Tables 2 and 3, and the high pressure results are presented in Table 4. Two or more depth profiles were typically measured on each sample, and the diffusion coefficients reported in Tables 2, 3, and 4 represent the mean of values determined from these repeat analyses. Diffusion coefficients obtained from different profiles on the same sample agreed to better than 25% in nearly every case, and always to better than 40%. Much of the scatter in diffusion coefficients can be attributed to error in the measurement of SIMS pit depths, which typically led to an uncertainty in D of 20%.

A time series study was performed at 1 atm and 1,200 °C, and the results are plotted in Fig. 2. Diffusion coefficients from these experiments, with anneal times ranging from 119 to 456 h, are in excellent agreement, and the total range of diffusion coefficients among the experiments is similar to the interprofile variation within a single sample. This demonstrates that diffusion coefficients are independent of anneal time and is consistent with transport by volume diffusion.

There appears to be no significant effect on Ce diffusion of the simultaneous transport of Yb. Diffusion coefficients determined from experiments in which Ce was the only rare earth element present in the tracer layer were indistinguishable from those determined from experiments in which both Ce and Yb diffused into the diopside.

One experiment was performed to measure the diffusivity of Yb with the oxygen fugacity held 4 log units above the QFM buffer at 1,200 °C. The diffusion coefficient determined from this experiment was more

Table 2 Summary of 1 atm run conditions and diffusion data for Ce and Yb

Run no.	T (°C)	Anneal time (h)	log f_{O_2}(bar)	Diffusion coefficients (10^{-21} m^2/s)	
				Ce	Yb
CeYb6	1,300	23.2	–7.8	31.9 ± 11.5	537 ± 96
CeYb9	1,275	76.9	–7.7	25.0 ± 10.1	465 ± 86
CeYb3	1,250	74.7	–7.9	11.5 ± 2.8	143 ± 37
CeYb2	1,250	190.8	–7.9	6.83 ± 1.35	142 ± 60
CeYb7	1,225	183.3	–8.5	5.83 ± 2.26	130 ± 27
CeYb8	1,200	455.6	–8.6	2.53 ± 0.47	43.7 ± 8.6
CeYb10	1,200	235.0	–8.6	4.45 ± 0.92	54.7 ± 11.3
CeYb4	1,200	191.4	–8.4	4.01 ± 1.42	49.8 ± 17.7
Ce1	1,200	118.9	–8.4	4.53 ± 2.10	–
Yb1	1,200	145.6	–4.5	–	158 ± 34
CeYb12	1,175	170.3	–8.4	–	27.0 ± 8.8
Ce3	1,150	577.8	–9.1	0.68 ± 0.12	–
CeYb1	1,150	455.6	–9.2	0.62 ± 0.36	24.2 ± 9.1
CeYb11	1,125	477.8	–9.7	–	13.7 ± 2.6
CeYb5	1,100	425.0	–9.8	–	4.62 ± 1.6
CeYb15	1,050	794.4	–10.5	–	1.41 ± 0.20

Table 3 Summary of 1 atm run conditions and diffusion data for La, Nd, and Dy

Run no.	T (°C)	Anneal time (h)	log f_{O_2}(bar)	Diffusion coefficients (10^{-21} m^2/s)		
				La	Nd	Dy
LaNdDy4	1,300	25.1	–7.3	21.5 ± 7.6	38.1 ± 13.0	190 ± 65
LaNdDy2	1,275	76.9	–7.7	10.0 ± 4.0	22.5 ± 9.2	170 ± 69
LaNdDy10	1,250	95.5	–7.9	4.46 ± 3.10	10.2 ± 7.1	97.2 ± 43.0
LaNdDy7	1,250	42.5	–8.2	–	–	72.8 ± 49.2
LaNdDy1	1,200	455.6	–8.6	1.82 ± 0.62	2.95 ± 1.00	17.9 ± 6.1
LaNdDy3	1,200	235.0	–8.6	–	–	24.8 ± 9.5
LaNdDy6	1,175	170.3	–8.4	–	–	12.4 ± 6.0
LaNdDy9	1,100	882.2	–9.8	–	–	1.30 ± 0.76

Table 4 Summary of high pressure run conditions and diffusion data for Ce and Yb

Run no.	Capsule	T (°C)	P (GPa)	Duration (h)	D_{Ce} (10^{-21} m^2/s)	D_{Yb} (10^{-21} m^2/s)
B588	Graphite	1,450	1.8	25.1	183 ± 136	3100 ± 1570
B584	Graphite	1,350	1.3	20.2	–	665 ± 224
C163	Graphite	1,350	1.5	70.0	33 ± 19	322 ± 176
C177	Graphite	1,350	2.5	72.2	–	202 ± 73
C207	Graphite	1,300	1.5	67.2	–	166 ± 89
B596	Graphite	1,250	1.8	75.8	–	60 ± 34
B475	Pt	1,450	1.8	68.1	66 ± 29	781 ± 355
B474	Pt	1,350	1.8	68.1	10 ± 7	71 ± 34
B553	AuPd	1,350	1.8	42.2	–	73 ± 23

than a factor of 3 higher than in the three experiments performed at the QFM buffer, suggesting a positive dependence of D on f_{O_2} (Fig. 3). This is important because it suggests that the point defects responsible for diffusion of the REE are those present to compensate the charge of an impurity whose valence is sensitive to oxygen fugacity. As discussed below, the positive dependence of D on f_{O_2} is consistent with diffusion by a vacancy mechanism, with the dominant vacancies being those present to compensate Fe^{3+} impurities on M1 sites.

Figure 4 shows an Arrhenius plot summarizing the results of diffusion experiments performed along the QFM buffer at 1 atm. The diffusion data for each element are consistent with an Arrhenius relationship, $D = D_0 e^{-E/RT}$, where D_0 is the pre-exponential factor, E is the activation energy, and R is the gas constant. Values of D_0 and E were determined by linear least squares regression and are listed in Table 5. Diffusion coefficients among the rare earth elements are strongly dependent on ionic radius, with D_{Yb} (0.0985 nm in eightfold coordination) being ~3 times greater than D_{Dy} (0.103 nm), ~20 times greater than D_{Nd} (0.111 nm) and D_{Ce} (0.114 nm), and ~35 times greater than D_{La} (0.116 nm). This trend of decreasing diffusivity with increasing ionic radius is consistent with an elastic strain model for diffusion, as discussed below. In the high pressure experiments, a systematic difference in diffusion rates is observed between samples annealed in contact with Pt or AuPd and those annealed in contact with

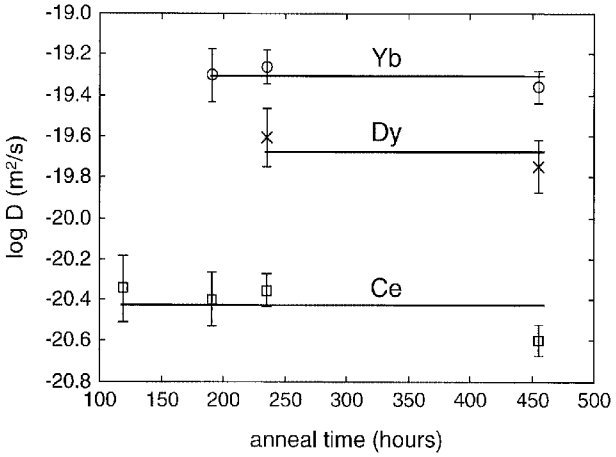

Fig. 2 Time series showing diffusion coefficients for Yb, Dy, and Ce versus run duration, for experiments run at 1 atm and 1,200 °C. The diffusion coefficient for each element is independent of anneal time, a necessary condition for mass transport by volume diffusion

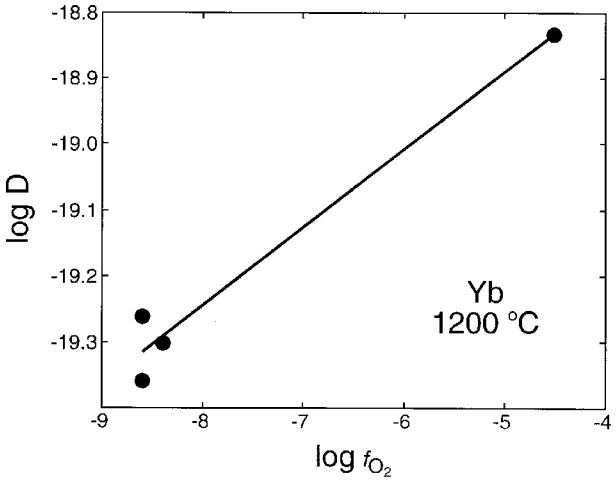

Fig. 3 Plot of $\log D_{Yb}$ versus oxygen fugacity at 1,200 °C. The positive dependence of Yb diffusivity on oxygen fugacity is consistent with a vacancy mechanism for diffusion, with the dominant vacancies being those present to electrically compensate Fe^{3+}

graphite. This difference appears to be related to loss of Fe from diopside crystals that were annealed in noble metal capsules, and because of this complication we considered only data from runs in graphite capsules when evaluating the influence of pressure on diffusion of Ce and Yb.

Diffusion coefficients determined from experiments run in noble metal capsules are internally consistent – a sample run in a sealed AuPd inner capsule within a mol ten NaCl medium yielded the same value of D_{Yb} as a run in which the sample was wrapped in Pt foil and surrounded by graphite. Samples annealed within a molten NaCl confining medium should have experienced isostatic stress, and the consistency among these results

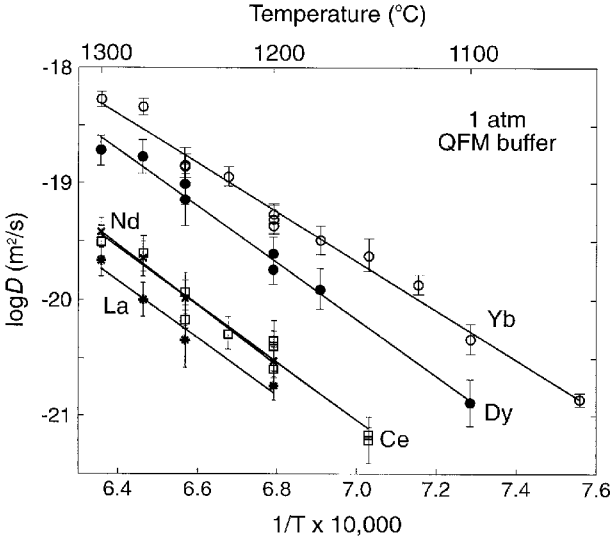

Fig. 4 Arrhenius plot showing diffusion coefficients versus T^{-1} for experiments run at 1 atm total pressure, with oxygen fugacity controlled near the QFM buffer. *Open circles* Yb; *filled circles* Dy; *crosses* Nd; *open squares* Ce; *asterisks* La. Arrhenius parameters obtained by linear least squares regression are given in Table 5

Table 5 Arrhenius parameters ($D = D_0 e^{-E/RT}$) for diffusion at 1 atm along the QFM buffer. Uncertainties (1σ) were determined from the linear regression

Element	$\log_{10} D_0$ (m^2/s)	E (kJ/mol)
Yb	-4.64 ± 0.42	411 ± 12
Dy	-3.31 ± 1.44	461 ± 41
Nd	-2.95 ± 2.64	496 ± 77
Ce	-4.10 ± 1.08	463 ± 31
La	-4.22 ± 2.66	466 ± 78

indicates that the deviatoric stresses experienced by samples held within a graphite confining medium have no significant effect on the rate of REE diffusion. Samples that were held in direct contact with graphite, with no intervening Pt foil, also yield internally consistent diffusion coefficients, but D_{Ce} and D_{Yb} from these runs are a factor of 3–4 higher than in runs performed in noble metal containers. We measured SIMS depth profiles of ^{56}Fe in two samples that had been annealed in contact with a noble metal (B474 and B553), one sample annealed in a graphite capsule, and several samples annealed at 1 atm in open Pt capsules. The secondary ion voltage was displaced by –110 V to reduce molecular interferences. No Fe loss was found in samples annealed at 1 atm or at high pressure in graphite capsules, but both samples annealed in noble metal containers experienced significant Fe loss. In these samples the Fe concentration decreases smoothly toward the interface with the noble metal (Fig. 5), with a relative Fe loss of 90% immediately adjacent to the interface. There was no perceptible change in Si or Ca concentration along the Fe loss profile. The Fe profiles conform to an error

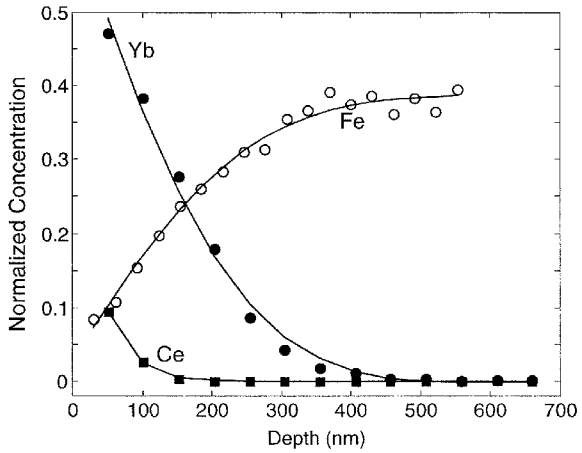

Fig. 5 SIMS depth profiles for Fe, Yb, and Ce from a high pressure experiment performed in a Pt container (B474 – 1,350 °C, 1.8 GPa). Concentrations refer to element/^{30}Si intensity ratios. Relative loss of Fe from the diopside at the Pt interface is ~90%

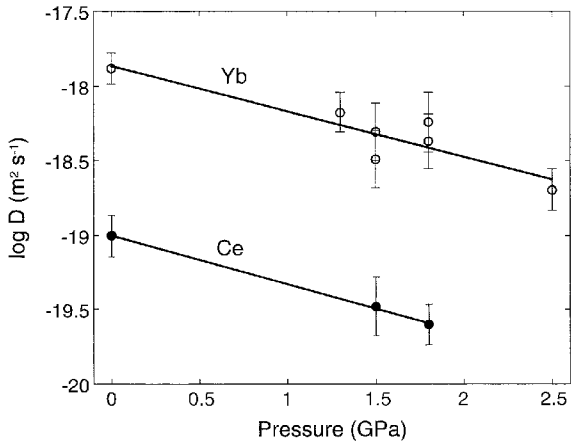

Fig. 6 Plot of Yb and Ce diffusion coefficients versus pressure, with all data corrected to 1,350 °C. Only high pressure experiments performed in graphite capsules are shown. The 1 atm data are shown as a single point representing the mean value of D, with *error bars* reflecting one standard deviation of the mean

function solution to the diffusion equation, and the diffusion coefficients of $7.0 \pm 3.2 \times 10^{-20}$ m^2/s (B474) and $4.9 \pm 2.0 \times 10^{-20}$ m^2/s (B553) are very similar to the Yb diffusion coefficients obtained from the same experiments. The noble metal capsules did not contain any elements that may have served as a counterflux for Fe, and thus the loss of Fe from the diopside must have been compensated by the introduction of M1 vacancies. The introduction of REE onto M2 sites may have helped to balance the effective negative charge of these M1 vacancies.

The reduction in Ce and Yb diffusion rates in experiments performed with noble metal capsules may be related to changes in defect chemistry associated with the loss of Fe. The positive dependence of D on oxygen fugacity observed in the 1 atm experiments suggests that the dominant vacancies in the Kunlun Mountains diopside are those that have been created to compensate Fe^{3+} on M1 sites. Loss of Fe^{3+} and associated M2 vacancies would lead to a decrease in diffusivity by reducing the number of vacant sites available for Ce and Yb atoms to hop to.

Diffusion data from the high pressure experiments performed in graphite capsules and from 1 atm anneals performed along the QFM buffer were multiply regressed against P and T^{-1} (Figs. 6 and 7). The data are consistent with an Arrhenius relationship $D = D_0 e^{-(E+PV)/RT}$, where V is the activation volume. Values of D_0, E, and V determined from the regressions are listed in Table 6. The values of D_0 and E are nearly identical to those determined from the 1 atm data set alone, but are determined with slightly better precision. In Fig. 7 the 1 atm and high pressure diffusion data are shown together on a plot of log D vs. inverse temperature, with the high pressure diffusion coefficients adjusted to 1 atm pressure. The 1 atm and high pressure data are in excellent agreement, and there are no changes in slope that

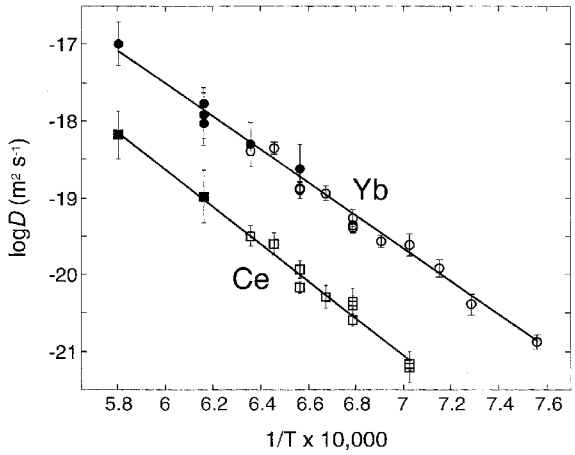

Fig. 7 Arrhenius plot comparing high and low pressure diffusion data for Yb and Ce. The high pressure data (*filled circles*) have been corrected to 1 atm pressure using the activation volumes determined from multiple linear regression of the data (Table 6; values uncorrected for oxygen fugacity)

would suggest a change in diffusion mechanism between 1,050 and 1,450 °C.

Activation volumes for Ce and Yb are similar, and over the temperature range investigated amount to a decrease in diffusivity by nearly an order of magnitude as pressure is increased from 1 atm to 2.5 GPa. The reported uncertainties in the activation volumes (Table 6) are those determined from statistical fits to the data, and take into account estimated uncertainties in measurement of the diffusion coefficients, pressure, and tempera ture. The temperature gradient across our high pressure sample assemblies is ~20 °C between the thermocouple junction and the center of the capsule, where the coated surface of the diopside was carefully placed. Our

Table 6 Arrhenius parameters ($D = D_0 e^{-(E+PV)/RT}$) for pressures of 0.1 MPa to 2.5 GPa and temperatures of 1,050–1,450 °C. Uncertainties (1σ) were determined from the multiple linear regression. The last three columns are: activation energy calculated for constant oxygen fugacity, assuming that the diffusion coefficient is proportional to f_{O_2} raised to the $m = 2/11$ power; activation volume calculated from 1 atm and high pressure data, with no f_{O_2} correction; and activation volume calculated for constant oxygen fugacity, assuming $m = 2/11$

Element	$\log_{10} D_0$ (m^2/s)	E (kJ/mol) QFM buffer	E (kJ/mol) f_{O_2} constant	V (cm^3/mol)	V (cm^3/mol) f_{O_2} constant
Yb	−4.63 ± 0.39	411 ± 11	321 ± 11	9.5 ± 2.0	9.0 ± 2.0
Ce	−4.12 ± 0.94	463 ± 27	373 ± 27	10.2 ± 3.2	8.9 ± 3.2

experience with phase equilibrium experiments using the MIT piston-cylinder assemblies suggests that the temperature in the center of the charge can be reproduced within < 20 °C in repeated experiments (e.g., Van Orman and Grove 2000). We made no correction for the effect of pressure on thermocouple emf, but this effect is expected to be small (< 15 °C) under the P–T conditions of our experiments (Williams and Kennedy 1969). Considering the various sources of error, 20 °C is taken to be a reasonable estimate of the temperature uncertainty in the piston-cylinder experiments. The oxygen fugacity in the piston-cylinder experiments, if buffered by the presence of graphite in equilibrium with a COH fluid, is very near that of the QFM buffer at 1 atm (Ulmer and Luth 1991). When the data are corrected to constant oxygen fugacity using our results for the f_{O_2} dependence of the Yb diffusion coefficient and the Ulmer and Luth (1991) calibration of the graphite–COH buffer (taking into account the pressure dependence of the buffer), the activation volume for Yb decreases from 9.5 to 9.0 cm^3/mol, and the activation volume for Ce decreases from 10.2 to 8.9 cm^3/mol. These corrected values are likely to be underestimated slightly because our experiments were performed in a H_2O free system, with lower H_2 fugacity and slightly higher oxygen fugacity than in the Ulmer and Luth (1991) experiments, which were buffered by the hematite–magnetite–H_2O equilibrium.

The activation volumes we report are somewhat higher than the activation volume of 1–3.5 cm^3/mol for Mg self-diffusion in olivine (Chakraborty et al. 1994) but similar to the activation volume of ~8–10 cm^3/mol for divalent cation diffusion in aluminosilicate garnets (Chakraborty and Rubie 1996; Ganguly et al. 1998a). The only previous determination of the pressure dependence of diffusion in pyroxene was made by Sneeringer et al. (1984), who found an apparent negative activation volume for Sr diffusion in synthetic diopside. Sneeringer et al. (1984) also found a large apparent anisotropy in the activation volume, with diffusion parallel to a and b having a stronger pressure dependence than diffusion parallel to c. There is significant scatter in the high pressure data of Sneeringer et al. (1984), and a small positive activation volume for the c direction (the same crystallographic direction investigated in this study) is within the uncertainty in the diffusion measurements. The high pressure experiments of Sneeringer et al. (1984) were performed by placing two diopside crystals, one doped with Sr and the other undoped, together within the high pressure cell. We have attempted high pressure diffusion anneals using a similar geometry, but had difficulty retrieving the flat, polished surfaces of the diopside crystals after the experiment. We do not know the reason for the anomalous activation volumes found by Sneeringer et al. (1984), but one possibility is that they are experimental artifacts related to preparation and retrieval of the diopside surfaces.

Comparison with other pyroxene diffusion data

The only previous experimental study of rare earth element diffusion in diopside was that of Sneeringer (1981) and Sneeringer et al. (1984), who measured Sm diffusion rates in a synthetic diopside single crystal. Figure 8 shows an Arrhenius plot comparing the Sm diffusion data with our 1 atm data for La, Ce, Nd, Dy, and Yb. On the basis of the relationship observed in our data set between D and ionic radius, we would expect D_{Sm} to be less than D_{Dy} and greater than D_{Nd}. The 1 atm Arrhenius curve of Sneeringer (1981) is slightly lower

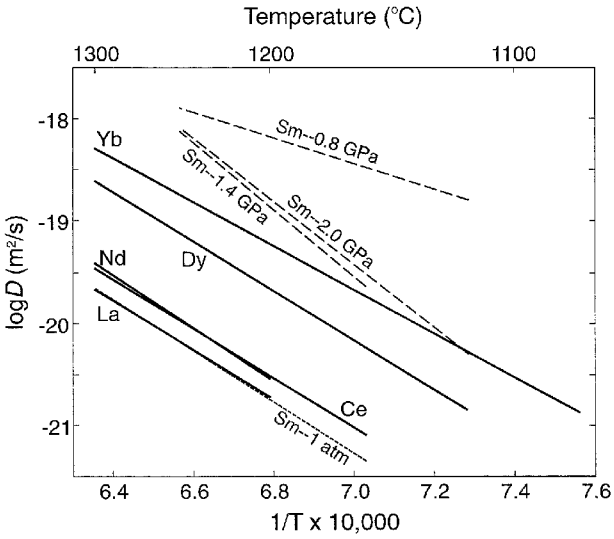

Fig. 8 Arrhenius plot comparing REE diffusion data from this study (at 1 atm) with Sm diffusion data for synthetic diopside. The 1 atm Sm diffusion data are from Sneeringer (1981) and the high pressure data are from Sneeringer et al. (1984)

than our curve for Nd, but given the relatively large scatter in the Sm diffusion data (up to an order of magnitude at a given temperature), this is considered to be in reasonable agreement with our data. The high pressure Sm data of Sneeringer et al. (1984) are about an order of magnitude higher than our data for Dy at 1 atm, and the discrepancy increases if our data are corrected to higher pressures. As mentioned above, it is possible that difficulties with surface preparation and retrieval may account for the high apparent diffusion rates in the high pressure experiments of Sneeringer et al. (1984).

Figure 9 shows a comparison of our 1 atm diffusion data for the rare earth elements with diffusion data for other elements in diopside. Arrhenius curves for most elements, including the REE, U, Th, Ca, and O, fall within a narrow band spanning about two orders of magnitude at a given temperature. Lead and strontium (in natural diopside crystals) fall about two orders of magnitude above this band, and Si falls below. Much of the variation in diffusivity among these elements may be explained as a consequence of the different sites that the ions occupy [the tetrahedral site in diopside has a much deeper energy well than the M1 or M2 site (Smyth and Bish 1988), which probably explains the slow diffusivity of Si relative to cations that partition onto the metal sites] and the size and charge of the ion relative to the ideal size and charge of the site. Diffusion rates are also influenced by the composition of the pyroxene. Strontium diffusion in natural diopside crystals, with the dominant impurity being Fe at the level of 1.5 wt% FeO*, is two orders of magnitude faster than Sr diffusion in nominally pure synthetic diopside crystals (Sneeringer et al. 1984). Calcium self-diffusion rates in natural diopside crystals containing ~1–2 wt% FeO are also faster than in pure synthetic diopside, by about an order of magnitude (Dimanov et al. 1996). In contrast to the relatively large compositional dependence of diffusion found by Sneeringer et al. (1984) and Dimanov et al. (1996) for Sr and Ca diffusion, Cherniak (1998a) found similar diffusion rates for Pb in two natural clinopyroxene crystals containing ~1 wt% and ~17 wt% FeO, respectively. Although further experimental work must be done in order to characterize the influence of pyroxene composition on diffusion rates, an interpretation consistent with existing data is that cation diffusion rates are reduced significantly only when the Fe concentration is quite low (less than ~1 wt%). This would perhaps imply that Fe^{3+} and associated cation vacancies become saturated at relatively low Fe contents, although the existing data set does not allow any definitive conclusion to be reached on this point.

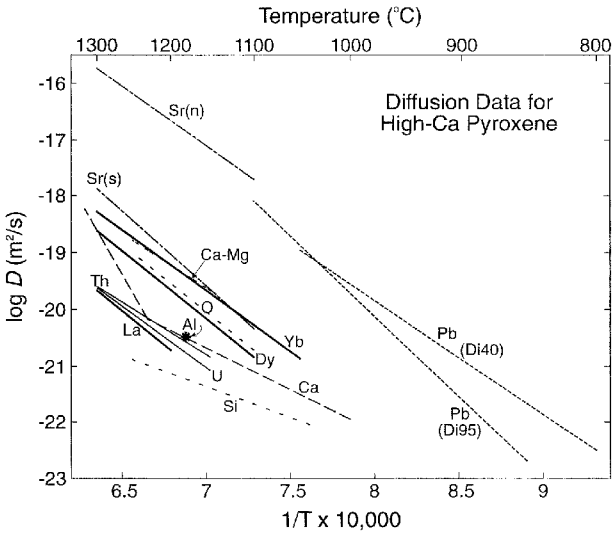

Fig. 9 Arrhenius plot of cation diffusion data in high-Ca clinopyroxene. References for the data are as follows: Sr [in both natural (n) and synthetic (s) diopside crystals] and Sm (synthetic) – Sneeringer et al. (1984); Pb – Cherniak (1998a); Ca – Dimanov and Jaoul (1998); Ca–Mg interdiffusion – Brady and McCallister (1983); O – Ryerson and McKeegan (1994); Al – Sautter et al. (1988); U and Th – Van Orman et al. (1998); Si – Béjina and Jaoul (1996); Yb, Dy, and La – this study

Discussion

Coupled element exchange during "tracer" diffusion

Coupled substitution is required to balance the extra positive charge that is introduced when a trivalent rare earth element is exchanged with a divalent cation on the diopside M2 site. Unfortunately we cannot directly infer the coupled substitution responsible for the uptake of REE in our experiments. The concentration of REE in the diopside is on the order of a few thousand parts per million at most, and at these low abundances it is not possible to resolve coupled variations in major element concentration that would indicate which substitution is taking place. However, because the tracer layer contained only rare earth element oxides, with no charge balancing species such as Al or Na present, it is likely that the introduction of REE into the diopside in our experiments involved an Eskola-type exchange, with charge balance achieved through the formation of vacancies on M1 or M2 sites. Two possible exchange reactions can be written as follows:

$$REE_2O_3 + 2Ca^{\times}_{M2} + Mg^{\times}_{M1} \rightarrow 2REE^{\cdot}_{M2} + V''_{M1} + MgO + 2CaO \quad (2)$$

or,

$$REE_2O_3 + 3Ca^{\times}_{M2} \rightarrow 2REE^{\cdot}_{M2} + V''_{M2} + 3CaO \quad (3)$$

using Kröger–Vink notation (e.g., Kröger 1974). In this notation X^Z_Y refers to an element X or vacancy V on a crystallographic site Y, with Z referring to the excess charge relative to that of the normally occupied site. A dot (˙) denotes one excess positive charge, a prime (′) stands for one excess negative charge, and a cross (×) indicates that the site has no excess charge. Eq. (2) describes the substitution of two REE^{3+} ions for two Ca^{2+} ions on the M2 site, with the formation of a

vacancy on the M1 (Mg) site to balance the charge. In this reaction Mg and Ca are transported out of the diopside crystal and deposited on the surface as MgO and CaO. The reaction described by Eq. (3) is similar but involves formation of a vacancy on M2 (Ca) rather than M1. We cannot rule out other exchanges, such as a Tschermak's (REEAl–CaSi) or jadeite (REENa–CaCa) type substitution. However, because no Na or Al is available in the tracer layer in our experiments, such exchanges would necessarily be accompanied by a net decrease in the number of lattice units in the diopside crystal, and outward transport of Si and other components. We consider this unlikely, because the self-diffusivity of Si in diopside (Béjina and Jaoul 1996) is an order of magnitude slower than the La diffusivity we have measured and more than two orders of magnitude slower than Yb. If a Tschermak's or jadeite substitution were responsible for uptake of REE in our experiments, we would expect transport to be limited by diffusion of Si, and rare earth element diffusion profiles to all be of similar length. The fact that we observed large differences in diffusivity among the REE indicates that transport is limited by the mobility of the rare earth elements themselves. It is possible that Si evaporated from the diopside surface (in the 1 atm anneals) or formed melt precipitates within the diopside crystal, rather than diffusing out of the crystal, but as noted above there was no optical evidence for this in any of the annealed samples.

There is reason to prefer REE incorporation via Eq. (2) rather than Eq. (3), because the latter reaction involves the formation of M2 vacancies that would lead to an enhancement in REE diffusion rates. If Eq. (3) were the dominant reaction, we would expect to see strong curvature in the erf^{-1} diffusion profiles, with the slope increasing with distance from the diffusion interface (i.e., with decreasing REE concentration). This is not observed, and none of the diffusion profiles show any evidence of the diffusion coefficient being dependent on REE concentration.

Diffusion mechanism

The positive dependence of D_{Yb} on oxygen fugacity is consistent with diffusion by a vacancy mechanism. Under oxidizing conditions excess oxygen may be incorporated into the diopside structure, creating cation vacancies that are electronically compensated by Fe^{3+} on M1 sites ($Fe^{\cdot}_{M1}$). This reaction can be described by the following equation:

$$8Fe^{\times}_{M1} + 2O_2 = 4O^{\times}_{O} + V''_{M2} + V''_{M1} + V''''_{Si} + 8Fe^{\cdot}_{M1} \quad (4)$$

with the corresponding mass action law:

$$\left[V''_{M2}\right]\left[V''_{M1}\right]\left[V''''_{Si}\right]\left[Fe^{\cdot}_{M1}\right]^8 = K\left[Fe^{\times}_{M1}\right]^8 f^2_{O_2} \quad (5)$$

If the electroneutrality condition $\left[Fe^{\cdot}_{M1}\right] = 2\left[V''_{M2}\right] + 2\left[V''_{M1}\right] + 4\left[V''''_{Si}\right]$ is satisfied and the concentrations of M1, M2, and Si vacancies are approximately equal [as would be the case if most vacancies were produced by the reaction described by Eq. (4)], then $\left[V''_{M2}\right] \propto f^m_{O_2}$, with $m = +2/11$. If diffusion of the rare earth elements is governed by M2 vacancies, the diffusion coefficients should have the same proportionality with f_{O_2}. Our preliminary investigation of the f_{O_2} dependence of Yb diffusivity at 1,200 °C suggests that $m \approx 0.13$, slightly lower than the value of ~0.18 predicted from the point defect model. Cherniak (2001) has investigated the influence of f_{O_2} on diffusion of Pb in four different clinopyroxene samples spanning a wide range of compositions, and one enstatite sample. A positive dependence of the diffusion coefficient on f_{O_2} was observed in all cases, with $m \approx 0.18$ for a near end member diopside sample. In contrast to the results of Cherniak (2001) for Pb and our preliminary result for Yb, Dimanov and coworkers have found that diffusion of Ca in diopside is *inversely* proportional to f_{O_2}, with $m \approx -0.19$. This result suggests that Ca diffuses by an interstitial rather than a vacancy mechanism; the inverse dependence on oxygen fugacity is consistent with a point defect model in which Ca interstitials are formed in response to oxygen desorption and associated reduction of $Fe^{\cdot}_{M1}$ to $Fe^{\times}_{M1}$ (Jaoul and Raterron 1994; Dimanov and Jaoul 1998). It appears that the energy required for an M2 cation to move to an adjacent vacancy is not very different from that required for a jump to an M3 or M4 interstitial site, and as a result the diffusion mechanism that an ion prefers is very sensitive to its size and charge.

The diffusion coefficient measured in annealing experiments can be related to atomic jump parameters by the following equation (e.g., Flynn 1972):

$$D = n\gamma a^2 f v_O \exp\left(\frac{S_m}{R}\right)\exp\left(\frac{-(E_m + PV_m)}{RT}\right), \quad (6)$$

where n is the mole fraction of vacancies or interstitial sites that govern diffusion, γ is a geometrical factor, a is the atomic jump distance, f is a correlation factor, and v_o is the jump attempt frequency (which is close to the vibrational frequency of an atom in its lattice site). S_m, E_m, and V_m are the entropy, energy, and volume of motion, respectively. Because our 1 atm experiments were performed along the QFM buffer rather than at constant oxygen fugacity, the apparent activation energies we have measured for diffusion of the REE do not represent motion energies alone, but include the influence of f_{O_2} on diffusivity. At constant f_{O_2} the activation energies for the REE would be less by mH_{QFM}, where H_{QFM} is the enthalpy of the QFM reaction, equal to +493 kJ/mol (Huebner 1971). If $m = +0.13$, the activation energy at constant f_{O_2} would be 64 kJ/mol less than along the QFM buffer, and if $m = +2/11$ as expected from the point defect model, the activation energy at constant f_{O_2} would be 90 kJ/mol less than along the QFM buffer. The activation energy at constant f_{O_2} is still not equivalent to the motion energy E_m, because there is also a contribution from the enthalpy of the vacancy formation reaction [Eq. (5)]. Unfortunately, the

thermodynamic data needed to estimate the enthalpy of this reaction are not available. Thermodynamic data do exist for a similar reaction in olivine (Nakamura and Schmalzried 1983; Simons 1986 as discussed in Chakraborty 1997), and the enthalpy is found to be very small – less than 20 kJ/mol – and may be either positive or negative depending on the coexisting phase that buffers the silica activity. The point defect model of Hirsch and Shankland (1993) gives a value of ~13 kJ/mol for Fo_{90} olivine with no solid buffers, and in the absence of data for pyroxene, we take this as an estimate for the enthalpy of the reaction expressed in Eq. (5). An estimate for the motion energy of Yb in diopside is then ~[411–(90 + 13)] = 308 kJ/mol. It is interesting to compare this to the calculated motion energy for Ca diffusion in diopside by a vacancy mechanism. Azough et al. (1998), using the Mott–Littleton approach with empirical interatomic pair potentials, found that the most favorable Ca jump requires ~190 kJ/mol. This is close to two thirds of the motion energy we estimate for Yb diffusion, which is the ratio expected if the motion energy is linearly proportional to the charge of the cation.

The activation volumes for Ce and Yb at constant temperature and constant f_{O_2}, 8.9 and 9.0 cm^3/mol, respectively, can be interpreted essentially as migration volumes. There must also be a contribution from the volume of the vacancy formation reaction, but this is certainly small and likely to be within the uncertainty in our activation volume measurements.

An elastic diffusion model

Because diffusion data for minerals remain sparse, there is considerable interest in obtaining an empirical or theoretical relationship that can be used to predict diffusion parameters for ions that have not yet been studied in the laboratory. In this section we introduce an elastic strain model for diffusion and discuss its application to diopside and other silicate minerals.

Relation between D and ionic radius

Mullen (1966) formulated a simple expression relating the motion energy of an impurity in an ionic solid to the difference between the ionic radius of the impurity and the ideal site radius. This model has had success in rationalizing cation diffusion trends in MgO, a simple stoichiometric close-packed oxide (Mortlock 1968), but to our knowledge no attempt has yet been made to apply the model to silicate materials. Blundy and Wood (1994) have shown that an elastic strain model is very successful in explaining trace element partitioning data, and the Mullen model for diffusion is based on a similar premise, in that the motion of an ion is assumed to be governed by elastic strain of the crystal lattice. In the Mullen model, ions are represented as hard spheres linked by Einstein springs. The motion energy is taken to be the work required to move ions into a configuration (the so-called saddle-point configuration) that allows motion of a jumping ion along a straight-line path to an adjoining vacancy (Mullen 1966). The work expended in moving the ions into the saddle-point configuration is assumed to be purely due to elastic strain and does not include small differences in Coulomb energy between the equilibrium configuration and the saddle-point configuration. With these assumptions, a relation between the motion energy and the ionic radius can be written as follows (combining Mullen's Eqs. 2 and 4):

$$E_m = E_m^\circ \left\{ 1 + 2 \left[\delta \left(1 - 1/\sqrt{2} \right)^{-1} - \delta \left(1 - 1/\sqrt{2} \right)^{-2} \right] \right\}. \quad (7)$$

The parameter E_m° in Eq. (7) refers to the motion energy for an ion with ideal radius, and δ is a size factor defined as $(r_i - r_{site})/r_o$, where r_i is the radius of the impurity ion, r_{site} is the ideal site radius, and r_o is the average cation–anion bond length for the site. The Mullen equation predicts a parabolic relation between the motion energy and the ionic radius for ions occupying a particular site. The maximum motion energy is predicted for an ion with $\delta = 0.147$. The REE in diopside have values of δ between 0.0440 (for La) and –0.0260 (for Yb), assuming an ideal M2 site radius of 0.105 nm (Blundy and Wood 1994) and an average M2–O bond length of 0.250 nm (Smyth and Bish 1988). If E_m° for a trivalent ion has a value of ~330 kJ/mol (estimated from the inferred motion energies for the REE, interpolated to $\delta = 0$), the motion energy is predicted to increase by ~140 kJ/mol from Yb to La. There does appear to be an increase in the apparent activation energy (and thus the motion energy) with increasing ionic radius, but the trend is poorly resolved because the uncertainties are large relative to the absolute differences in activation energy among the REE. For this reason it is not possible to determine whether there actually is a parabolic relation between the activation energy and the lattice misfit.

The relative variation in diffusivity among the rare earth elements at a particular temperature is much greater than the variation in activation energy, and the Mullen equation can be compared to our data more readily if it is recast in terms of D rather than E_m. This can be done provided that a relationship can be formulated between the pre-exponential factor (D_0) and ionic radius. In many materials, including silicate minerals (Hart 1981) and melts (Hofmann 1980), a positive correlation is found among D_0 and E. Zener (1952) showed that such a correlation is expected on theoretical grounds, if a large part of the energy expended during an atomic jump is due to elastic strain of the crystal lattice. In this case a relation between the motion entropy and the temperature coefficient of the bulk (or shear) modulus μ is expected, as described by the following equation:

$$\ln D_0 \propto S_m \approx -\{\partial(\mu/mu_\circ)/\partial T\} E_m. \quad (8)$$

D_0 is a composite term comprising several atomic jump parameters [the first six terms in Eq. (6), for extrinsic diffusion], but most of them are related to the

mineral structure and only S_m and v_o depend on the properties of the jumping ion. If it is assumed that variations in v_o among the REE are small and that variation in D_0 is due primarily to differences in S_m (in other words, that the jump attempt frequencies among the REE are similar, but that the success of a jump is determined by the size of the ion), then the Mullen equation [Eq. (7)] can be combined with the Zener relation [Eq. (8)] to give:

$$\ln D = \ln D^{\delta=0} - 2b\left[\delta\left(1-1/\sqrt{2}\right)^{-1} - \delta^2\left(1-1/\sqrt{2}\right)^{-2}\right], \quad (9)$$

where

$$b \approx \frac{E_m^\circ}{R}\left[\frac{\partial(\mu/\mu_\circ)}{\partial T} + \frac{1}{T}\right]. \quad (10)$$

Eq. (9) describes a parabola on a plot of ln$D$ vs. δ, with a minimum at $\delta = 0.147$. For the diopside M2 site, the minimum in diffusivity is predicted for an ion with radius ~0.142 nm. The REE are all much smaller than this "minimum diffusivity" radius and thus their diffusion coefficients are expected to decrease monotonically with increasing ionic radius. This prediction is in accord with the results of our experiments. Figure 10 shows our experimental results for diffusion of La, Ce, Nd, Dy, and Yb at 1 atm and 1,200 °C on a plot of ln D vs. δ. The curve through the data was obtained by a least squares fit to Eq. (9), with $\ln D^{\delta=0}$ and b as the only adjustable parameters. The parameter b controls the "tightness" of the parabola – the larger the value of b, the tighter the parabola – and $D^{\delta=0}$ determines the vertical placement of the curve. The parabola is not adjusted along the δ axis; its horizontal position on the plot is fixed by specifying the ideal M2 site radius (0.105 nm; Blundy and Wood 1994) and mean M2–O bond length (0.250 nm; Smyth and Bish 1988). The values of b and $D^{\delta=0}$ obtained from the fit are given in Table 7.

As shown in Fig. 10, the Mullen/Zener model (henceforth referred to as MZ) appears to provide an excellent description of REE diffusion rates in diopside at 1,200 °C. It also describes the temperature dependence of REE diffusion quite well (Fig. 11). The Arrhenius lines shown in Fig. 11 are not fits to the data but were obtained from the MZ model, as follows. The motion energy for each element is assumed to follow Eq. (7), with $E_m^\circ = 330$ kJ/mol. Because the diffusion data were obtained along the QFM buffer rather than at constant oxygen fugacity, the apparent activation energy (represented by the slope of the Arrhenius line) is taken to equal $(E_m^\circ + 90 + 13)$ kJ/mol. Relative values of $\ln D_0$ are given by Eq. (8), using the value of $-\partial(\mu/\mu_0)\partial T$ obtained from the fit of Eqs. (9) and (10) to the data at 1,200 °C. The Arrhenius curves obtained from the MZ model (Fig. 11) pass through nearly all of the data points for each element within error, and fit the data nearly as well as Arrhenius curves statistically fitted to the data by least squares regression (Fig. 4). The MZ model thus appears to provide a useful means for estimating the Arrhenius parameters of rare earth elements (as well as other trivalent elements that par-

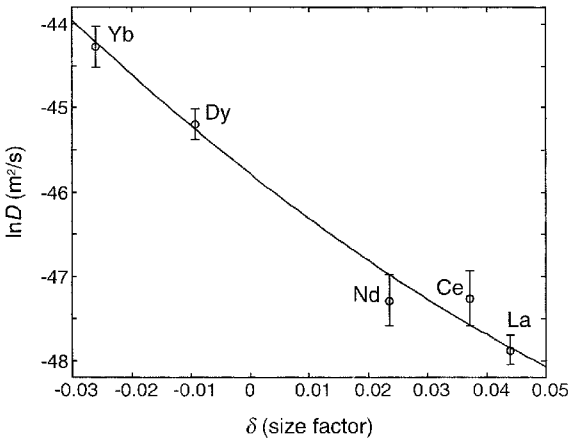

Fig. 10 Plot of ln$D$ versus the ionic size factor $\delta = (r_i - r_{site})/r_o$ for REE diffusion in diopside at 1,200 °C and 1 atm. r_i is the radius of the trivalent ion in eightfold coordination (Shannon 1976), r_{site} is the ideal site radius (0.105 nm; Blundy and Wood 1994), and r_o is the average cation–anion bond length (0.250 nm; Smyth and Bish 1988). The curve is a least squares fit to Eq. (7) with ln $D^{\delta=0}$ and b as the only adjustable parameters

Table 7 Parameters in Mullen/Zener (MZ) model

Column notes	r_{site} (nm)	r_0 (nm) a	$\partial(\mu/\mu_\circ)/\partial T$ ($\times 10^4$ K^{-1})	E_m°(kJ/mol) b	$\ln D^{\delta=0}$ c	b c	b* d
Diopside, 3+[e]	0.105[f]	0.250	–1.3[g]	330	–45.78	8.1	22
Zircon, 3+[h]	0.084[i]	0.220	–0.89[j]	670	–37.25	25	48
Anorthite, 2+[k]	0.120[f]	0.253	–	250	–41.48	2.1	–

[a]Values from Smyth and Bish (1988)
[b]Migration enthalpy at $\delta = 0$ (estimated from measured activation enthalpies)
[c]Determined from least squares fit to Eq. (7) of diffusion coefficients at 1,200 °C
[d]Calculated from Eq. (8)
[e]This study
[f]Ideal cation site radius (Blundy and Wood 1994)
[g]Anderson (1989, p. 105). Average of temperature derivatives of shear modulus and bulk modulus
[h]Cherniak et al. (1997a)
[i]Ideal site radius calculated as the mean cation–oxygen bond distance (r_0) minus the ionic radius of O^{2-} (0.138 nm)
[j]Bass (1995). Average of temperature derivatives of shear modulus and bulk modulus
[k]LaTourrette and Wasserburg (1998)

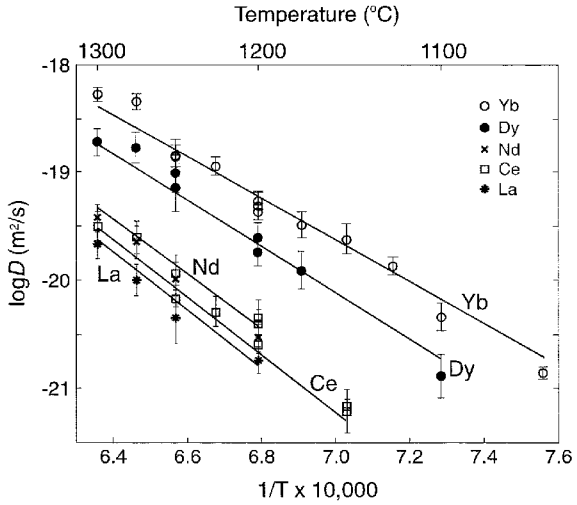

Fig. 11 Comparison of 1-atm diffusion data for the rare earth elements in diopside with Arrhenius curves predicted by the Mullen/Zener (MZ) model

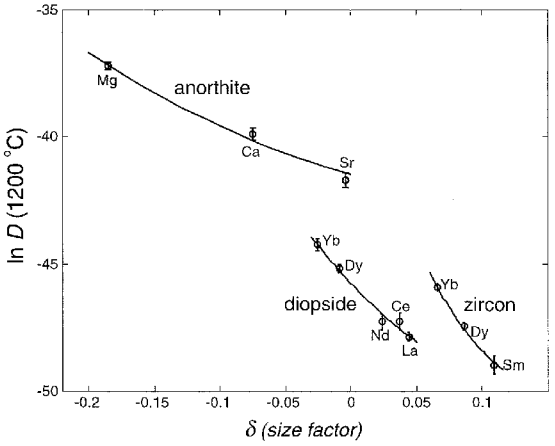

Fig. 12 Plot of $\ln D_{1473\ K}$ versus δ for alkaline earth elements in anorthite (LaTourrette and Wasserburg 1998), REE in zircon (Cherniak et al. 1997a), and REE in diopside (this study). Curves are least squares fits to Eq. (7); parameters obtained from the fits are given in Table 7

tition onto the M2 site) that have not yet been determined experimentally.

Diffusion data are also available for ions with a range of ionic radii in the silicate minerals zircon and anorthite. Diffusion coefficients for the REE in zircon (Cherniak et al. 1997a) and the alkaline earth elements in anorthite (LaTourrette and Wasserburg 1998) at 1,200 °C were fit to Eq. (9), and the results are shown in Fig. 12 along with those for the REE in diopside. The MZ model fits each data set quite well, and the relative values of b for each mineral (Table 7) are consistent with the relationship given in Eq. (10). The dependence of diffusivity on the size factor δ is greatest for zircon, which also has the largest motion energy (and the stiffest lattice). Diffusion in plagioclase has the weakest dependence on ionic radius among the three minerals, and the smallest activation energy for diffusion (as well as the most compliant lattice). These relationships are as expected for diffusion jumps accommodated by elastic strain of the crystal lattice. Although there is a general correspondence between the data and the predictions of the MZ model, there is one sense in which the model fails to quantitatively account for the data. The value of b predicted from Eq. (10) is a factor of ~2–3 greater than the value obtained from the fit to the diffusion data (Table 7). In other words, the dependence of diffusivity on ionic radius that is predicted from the MZ model, using experimentally determined motion energies and temperature derivatives of the elastic moduli, is greater than that observed in the diffusion data.

Although the MZ model appears to provide a good fit to the diffusion data for REE in diopside and zircon, and for alkaline earth elements in anorthite, it remains to be seen how generally the model applies. Aluminate and aluminosilicate garnets do not conform to the predictions of the MZ model – there is no significant variation in diffusion rates among the REE in pyrope (Van Orman 2000) and YAG (Cherniak 1998b) garnets despite the relatively stiff lattices of these materials.

Relation between D and ionic charge

The change in electrostatic energy required to move an ion to an adjacent vacant site in a solid is, to a first approximation, linearly related to ionic charge (e.g., Anderson and Stuart 1954). Taking the motion energy to be proportional to cation charge, a relationship among the diffusion coefficient D, ionic charge z, and size factor δ can be formulated as follows:

$$\ln D_z = \ln D_{z_{ref}}^{\delta=0} + b\left(1-\frac{z}{z_{ref}}\right) - 2b\left(\frac{z}{z_{ref}}\right)\left[\delta\left(1-1/\sqrt{2}\right)^{-1} - \delta^2\left(1-1/\sqrt{2}\right)^{-2}\right], \quad (11)$$

where b is as defined above [Eq. (10)] with E_m° equal to the motion energy for a cation with ideal radius and reference charge z_{ref}. This relationship can be compared to the diffusion data for divalent, trivalent, and tetravalent cations in diopside and zircon (Fig. 13) using the values of $\ln D_{z=3}^{\delta=0}$ and b determined from the REE diffusion data (Table 7). The diffusion data shown in Fig. 13 are corrected to $\delta=0$ using the relationship given by Eq. (11). The lines for diopside and zircon represent solutions to Eq. (11), and intersect $\ln D_{z=3}^{\delta=0}$ with a slope of $-b/3$. Although there is considerable scatter in the data for divalent ions in diopside and tetravalent ions in zircon, the model captures the general trends for the two minerals remarkably well. Eq. (11) predicts that a mineral in which D depends strongly on ionic radius should also exhibit a strong dependence of D on ionic charge. Diopside and zircon are consistent with this relationship; diffusion rates in

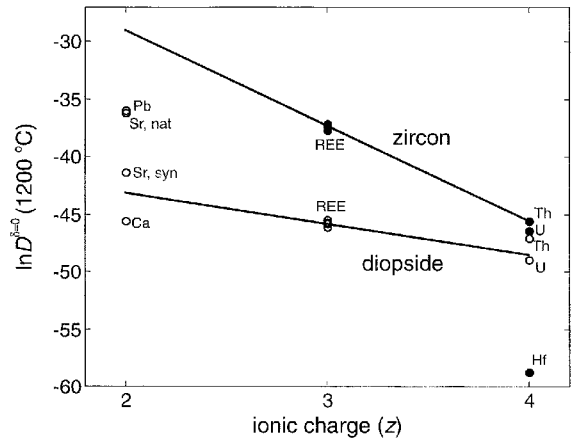

Fig. 13 Plot of $\ln D^{\delta=0}_{1473K}$ versus ionic charge for cations that partition onto the eightfold site in diopside and zircon. Diffusion coefficients are corrected to $\delta = 0$ using Eq. (10). The two *lines* on the plot are not fits to the data, but instead show trends predicted by Eq. (10), given $\ln D^{\delta=0}_{z=3}$ and b values determined from fits of the REE data to Eq. (7) (see Table 7). *Open circles* diopside; *filled circles* zircon. References for zircon diffusion data: REE – Cherniak et al. (1997a); U, Th and Hf – Cherniak et al. (1997b). References for diopside diffusion data: U, Th – Van Orman et al. (1998); REE – this study; Pb – Cherniak (1998a); Sr – Sneeringer et al. (1984); Ca – Dimanov and Jaoul (1998)

zircon are more sensitive to both size and charge than are diffusion rates in diopside.

Activation volume

An elastic strain model relating the activation volume and activation energy for diffusion was introduced by Keyes (1963) and has been discussed further by Flynn (1972) and Sammis et al. (1981). If the lattice distortions involved in the motion of an ion are perfectly elastic, then a lower bound on the motion volume is obtained by assuming that the lattice strain is purely shear, and an upper bound is obtained by assuming that strain is entirely dilatational. In the case of shear strain, the motion volume is given by:

$$V_m = E_m\left[\left(\frac{\partial(\ln G)}{\partial P}\right)_T - \frac{1}{K_T}\right]\left[1 - \left(\frac{\partial(\ln G)}{\partial(\ln T)}\right)_P - \beta T\right]^{-1} \quad (12)$$

where G is the shear modulus, K_T is the isothermal bulk modulus, and β is the coefficient of thermal expansion (Sammis et al. 1981). If the strain energy is assumed to be purely dilatational, then:

$$V_m = E_m\left[\left(\frac{\partial(\ln K_T)}{\partial P}\right)_T - \frac{1}{K_T}\right]\left[1 - \left(\frac{\partial(\ln K_T)}{\partial(\ln T)}\right)_P - \beta T\right]^{-1}. \quad (13)$$

Using values given by Anderson (1989) for the elastic moduli and their temperature and pressure derivatives, and the thermal expansion coefficient for diopside found in Fei (1995), Eqs. (12) and (13) yield estimates of 6.1 and 11.2 cm^3/mol, respectively, for the motion volume of Yb diffusion. These lower and upper bounds are in agreement with the measured activation volume (at constant oxygen fugacity) of 9.0 ± 2.0 cm^3/mol. For Ce, the experimental activation volume of 8.9 ± 3.2 cm^3/mol also falls within the predicted range of 7.0 to 12.8 cm^3/mol (for a Ce motion energy of 358 kJ/mol).

Applications of the data

The diffusion data presented above are applicable to a wide range of kinetic problems in high temperature geochemistry. Here the REE diffusion data are used to evaluate the length scale over which Nd isotopic heterogeneity can be maintained in the upper mantle, and to assess kinetic controls on REE uptake during basalt crystallization.

Isotopic heterogeneity

A large body of data from mid-ocean ridge basalts and ocean island basalts shows that the Earth's mantle is heterogeneous in isotopic composition (see Allègre et al. 1986; Zindler and Hart 1986; Hart et al. 1992; Hofmann 1997; and references therein). Hofmann and Hart (1978) argued for a mantle that is heterogeneous on a regional scale but homogeneous on a local (grain) scale. The original argument for grain-scale isotopic equilibrium was based on a diffusion data set that was quite sparse; in 1978 no experimental data were available for diffusion of radioisotopes in major upper mantle minerals. In 1984, Sneeringer et al. showed that diffusion of Sr in clinopyroxene is rapid enough at temperatures near the solidus of peridotite to easily maintain grain-scale $^{87}Sr/^{86}Sr$ homogeneity. Here we revisit the question of local equilibrium for Nd isotopes, using the present REE diffusion data set.

The calculations that follow assume that isotopic equilibration is governed by volume diffusion in the minerals. Mineral grains are assumed to maintain communication with each other through a network of high diffusivity paths (e.g., grain boundaries or melt tubules along three-grain junctions), with no intervening solid barriers to diffusional exchange between mineral grains. If clinopyroxene grains are "armored" by olivine or orthopyroxene, which can accommodate very little Nd, then isotopic equilibration may be significantly slower than in the case considered here. On the other hand, equilibration may be considerably faster if recrystallization or some other process acts to short-circuit volume diffusion.

Because diffusion of Nd is slower in clinopyroxene than in its other major host phase, garnet (Coghlan 1990; Ganguly et al. 1998b; Van Orman 2000), cpx exerts the primary control on the rate of equilibration of Nd isotopes. In garnet lherzolite at temperatures near the solidus (~1,450 °C at a pressure of 2.5 GPa) the diffusion coefficient for Nd in diopside is $\sim 2 \times 10^{-19}$ m^2/s, assuming an activation volume of 9 cm^3/mol (the dif-

fusion coefficient in pyrope garnet measured at 2.8 GPa and 1,450 °C is 4×10^{-19} m^2/s; Van Orman 2000). Under these conditions, a spherical cpx grain 5 mm in diameter can remain closed to Nd isotope exchange for only ~1 My. In this time, garnet and cpx with Sm/Nd ratios that differ by a factor of ~3–4 can maintain differences in $^{143}Nd/^{144}Nd$ of only $\sim10^{-6}$. This local-scale heterogeneity is very small compared to variations in $^{143}Nd/^{144}Nd$ of 10^{-4} to10^{-3} among MORB and OIB. Thus the common assumption that Nd isotopes are locally in equilibrium during melting of garnet lherzolite appears to be a good one.

Melting of eclogite may be a different story. The solidus of eclogite could be as low as 1,150 °C at 1.5 GPa pressure (e.g., Hirschmann and Stolper 1996), and under these conditions the diffusion coefficient for Nd in diopside is estimated to be $\sim2\times10^{-22}$ m^2/s [in pyrope garnet the diffusion coefficient would be two orders of magnitude higher (Van Orman 2000), assuming an activation volume of 8 cm^3/mol (Chakraborty and Rubie 1996)]. In this case significant isotopic disequilibrium can be maintained between 5 mm cpx and garnet grains for times on the order of a billion years, which could lead to differences in $^{143}Nd/^{144}Nd$ between cpx and garnet of $\sim10^{-3}$. This degree of grain-scale disequilibrium is quite large compared to the variation in Nd isotopic ratios observed in oceanic basalts. If eclogitic material makes an important contribution to basaltic magmas, the assumption of local isotopic equilibrium in the source may not be valid.

Because of the relatively large activation volumes for diffusion of the REE in clinopyroxene (9 cm^3/mol), the diffusion coefficients are expected to decrease significantly with depth along an adiabatic temperature gradient. High-Ca pyroxene is stable to ~15 GPa, i.e., within the mantle transition zone (e.g., Fei and Bertka 1999). Along a 0.4 °C/km adiabat, the Nd diffusion coefficient is expected to decrease by two orders of magnitude between 75 and 450 km depth– from 2×10^{-19} m^2/s at 1,450 °C, 75 km, to 3×10^{-21} m^2/s at 1,600 °C, 450 km. Diffusive transport of light REE in cpx will be effectively frozen at transition zone pressures, for time scales of 100 My or less. A 5-mm cpx grain under these conditions could remain closed to Nd isotopic exchange long enough to allow significant variations in $^{143}Nd/^{144}Nd$ to develop on the grain scale.

Disequilibrium REE uptake by clinopyroxene phenocrysts

Phenocrysts grown from silicate melts commonly exhibit disequilibrium features such as oscillatory zoning or sectoral enrichment. The underlying cause of disequilibrium may be related to boundary layer effects in the melt adjacent to the growing crystal (e.g., Albarède and Bottinga 1972) or to enrichment/adsorption at the crystal surface (Shimizu 1981; Watson and Liang 1995; Watson 1996). Preservation of the chemical zoning produced by either process is controlled by volume diffusion in the crystal. In the case of disequilibrium uptake due to surface enrichment phenomena, preservation of zoning depends on the value of the "growth" Peclet number, $Pe = Vl/D$, where V is the crystal growth rate, l is the enriched surface layer thickness, and D is the diffusion coefficient in the crystal (Watson 1996). Watson and Liang (1995) and Watson (1996) showed that perceptible disequilibrium uptake is possible if the Peclet number is greater than ~0.1. Phenocryst growth rates in basaltic lava lakes have been estimated to be in the range 5×10^{-13} to 10^{-11} m/s (Kirkpatrick 1977; Cashman and Marsh 1988). These growth rates are rapid enough to allow significant disequilibrium uptake of REE, even if the surface enrichment layer has a thickness on order of a single silicate monolayer (~0.5 nm). Phenocrysts growing at rates of 5×10^{-13} to 10^{-11} m/s at temperatures of 1,200–1,000 °C have Pe_{La} in the range 0.14–1,090 and Pe_{Yb} in the range 0.004–16. Thus, under conditions typical of basalt crystallization, La uptake by growing phenocrysts is expected usually to be a disequilibrium phenomenon, while uptake of Yb may take place under equilibrium or disequilibrium conditions depending on the temperature and phenocryst growth rate. At intermediate temperatures and crystallization rates, uptake of Yb and other heavy REE will take place under near-equilibrium conditions while uptake of La and other light REE is dominated by surface enrichment effects. Under such conditions the relative abundances and spatial distributions of REE in clinopyroxene phenocrysts are sensitive not only to variations in bulk and surface partitioning but to temperature and growth rate, and may provide a powerful record of the cooling and crystallization history of the host lava.

Acknowledgements This work was supported by grants from the National Science Foundation (OCE-9415968 and OCE-9731506) and by an NSF Graduate Research Fellowship. We thank George Harlow for providing the diopside specimens used in this work; Graham Layne for advice on SIMS depth profiling techniques; and Sumit Chakraborty and Daniele Cherniak for comments that improved the presentation of the manuscript.

References

Albarède F, Bottinga Y (1972) Kinetic disequilibrium in trace element partitioning between phenocrysts and host lava. Geochim Cosmochim Acta 36:141–156

Allègre CJ, Hamelin B, Provost A, Dupré B (1986) Topology in isotopic multispace and origin of mantle chemical heterogeneities. Earth Planet Sci Lett 81:319–337

Anderson DL (1989) Theory of the Earth. Blackwell Scientific, Oxford

Anderson OL, Stuart DA (1954) Calculation of activation energy of ionic conductivity in silica glasses by classical methods. J Am Ceram Soc 37:573–580

Azough F, Freer R, Wright K, Jackson R (1998) A computer simulation study of point defects in diopside and the self-diffusion of Mg and Ca by a vacancy mechanism. Mineral Mag 62:599–606

Bass JD (1995) Elasticity of minerals, glasses, and melts. In: Ahrens TJ (ed) Mineral physics and crystallography: a handbook of

physical constants. American Geophysical Union, Washington, DC, pp 45–63
Béjina F, Jaoul O (1996) Silicon self-diffusion in quartz and diopside measured by nuclear micro-analysis methods. Phys Earth Planet Inter 97:145–162
Blundy J, Wood B (1994) Prediction of crystal–melt partition coefficients from elastic moduli. Nature 372:452–454
Boyd FR, England JL (1960) Apparatus for phase equilibrium studies at pressures up to 50 kbars and temperatures up to 1750 °C. J Geophys Res 65:741–748
Brady JB, McCallister RH (1983) Diffusion data for clinopyroxenes from homogenization and self-diffusion experiments. Am Mineral 68:95–105
Cashman KV, Marsh BD (1988) Crystal size distribution (CSD) in rocks and the kinetics and dynamics of crystallization: II. Makaopuhi lava lake. Contrib Mineral Petrol 99:292–305
Chakraborty S (1997) Rates and mechanisms of Fe–Mg interdiffusion in olivine at 980°–1300 °C. J Geophys Res 102: 12317–12331
Chakraborty S, Rubie DC (1996) Mg tracer diffusion in aluminosilicate garnets at 750–850 °C, 1 atm and 1300 °C, 8.5 GPa. Contrib Mineral Petrol 122:406–414
Chakraborty S, Farver JR, Yund RA, Rubie DC (1994) Mg tracer diffusion in synthetic forsterite and San Carlos olivine as a function of P, T and f_{O2}. Phys Chem Mineral 21:489–500
Cherniak DJ (1998a) Pb diffusion in clinopyroxene. Chem Geol 150:105–117
Cherniak DJ (1998b) Rare earth element and gallium diffusion in yttrium aluminum garnet. Phys Chem Mineral 26:156–163
Cherniak DJ (2001) Pb diffusion in Cr diopside, augite, and enstatite, and consideration of the dependence of cation diffusion in pyroxene on oxygen fugacity. Chem Geol 177:381–397
Cherniak DJ, Hanchar JM, Watson EB (1997a) Rare-earth diffusion in zircon. Chem Geol 134:289–301
Cherniak DJ, Hanchar JM, Watson EB (1997b) Diffusion of tetravalent cations in zircon. Contrib Mineral Petrol 127:383–390
Christie DM, Carmichael ISE, Langmuir CH (1986) Oxidation-state of midocean ridge basalt glasses. Earth Planet Sci Lett 79:397–411
Coghlan RAN (1990) Studies of diffusional transport: grain boundary transport of oxygen in feldspars, strontium and the REE's in garnet, and thermal histories of granitic intrusions in south-central Maine using oxygen isotopes. PhD Thesis, Brown University, Providence, Rhode Island
Crank J (1975) The mathematics of diffusion, 2nd edn. Oxford University Press, Oxford
Dimanov A, Jaoul O (1998) Calcium self-diffusion in diopside at high temperature: implications for transport properties. Phys Chem Mineral 26:116–127
Dimanov A, Jaoul O, Sautter V (1996) Calcium self-diffusion in natural diopside single crystals. Geochim Cosmochim Acta 60:4095–4106
Doukhan N, Doukhan JC, Ingrin J, Jaoul O, Raterron P (1993) Early partial melting in pyroxenes. Am Mineral 78:1247–1257
Fei Y (1995) Thermal expansion. In: Ahrens TJ (ed) Mineral physics and crystallography: a handbook of physical constants. American Geophysical Union, Washington, DC, pp 29–44
Fei Y, Bertka CM (1999) Phase transitions in the Earth's mantle and mantle mineralogy. In: Fei Y, Bertka CM, Mysen BO (eds) Mantle petrology: field observations and high pressure experimentation. The Geochemical Society, Houston, pp 189–207
Flynn CP (1972) Point defects and diffusion. Oxford University Press, Oxford
Ganguly J, Cheng W, Chakraborty S (1998a) Cation diffusion in aluminosilicate garnets; experimental determination in pyrope–almandine diffusion couples. Contrib Mineral Petrol 131:171–180
Ganguly J, Tirone M, Hervig RL (1998b) Diffusion kinetics of samarium and neodymium in garnet, and a method for determining cooling rates of rocks. Science 281:805–807
Hart SR (1981) Diffusion compensation in natural silicates. Geochim Cosmochim Acta 45:279–291
Hart SR (1993) Equilibration during mantle melting: a fractal tree model. Proc Nat Acad Sci 90:11914–11918
Hart SR, Hauri EH, Oschmann LA, Whitehead JA (1992) Mantle plumes and entrainment: isotopic evidence. Science 256:517–520
Hays JF (1966) Lime–alumina–silica. Carnegie Inst Wash Yearb 65:234–236
Hirsch LM, Shankland TJ (1993) Quantitative olivine-defect chemical model: insights on electrical conduction, diffusion, and the role of Fe content. Geophys J Int 114:21–35
Hirschmann MM, Stolper EM (1996) A possible role for garnet pyroxenite in the origin of the "garnet signature" in MORB. Contrib Mineral Petrol 124:185–208
Hofmann AW (1980) Diffusion in natural silicate melts: a critical review. In: Hargraves RB (ed) Physics of magmatic processes. Princeton University Press, Princeton, pp 385–417
Hofmann AW (1997) Mantle geochemistry: the message from oceanic volcanism. Nature 385:219–229
Hofmann AW, Hart SR (1978) An assessment of local and regional isotopic equilibrium in the mantle. Earth Planet Sci Lett 38:44–62
Huebner JS (1971) Buffering techniques for hydrostatic systems at elevated pressures. In: Ulmer GC (ed) Research techniques for high pressure and high temperature. Springer, Berlin Heidelberg New York, pp 123–178
Ingrin J, Doukhan N, Doukhan JC (1991) High temperature deformation of diopside single crystal: 2. TEM investigation of the defect microstructures. J Geophys Res 96:14287–14297
Iwamori H (1993) Dynamic disequilibrium melting model with porous flow and diffusion controlled chemical equilibration. Earth Planet Sci Lett 114:301–313
Jaoul O, Raterron P (1994) High-temperature deformation of diopside crystal 3. Influences of pO_2 and SiO_2 precipitation. J Geophys Res 99:9423–9439
Keyes RW (1963) Continuum models of the effect of pressure on activated processes. In: Paul W, Warschauer DM (eds) Solids under pressure. McGraw-Hill, New York, pp 71–99
Kirkpatrick RJ (1977) Nucleation and growth of plagioclase, Makaopuhi and Alae lava lakes, Kilauea Volcano, Hawaii. Geol Soc Am Bull 88:78–84
Koga KT, Shimizu N, Grove TL (1999) Disequilibrium trace element redistribution during garnet to spinel facies transition. In: Gurney JJ, Gurney JL, Pascoe MD, Richardson SH (eds) Proceedings of the 7th International Kimberlite Conference, vol 1, pp 444–451
Kröger FA (1974) The chemistry of imperfect crystals, 2nd edn. North-Holland, New York
LaTourrette T, Wasserburg GJ (1998) Mg diffusion in anorthite: implications for the formation of early solar system planetesimals. Earth Planet Sci Lett 158:91–108
Mortlock AJ (1968) Divalent cation impurity diffusion in MgO. In: Mass transport in oxides. US Nat Bur Stand Spec Publ 296, pp 85–87
Mullen JG (1966) Theory of diffusion in ionic crystals. Phys Rev 143:658–662
Nakamura A, Schmalzried H (1983) On the nonstoichiometry and point defects of olivine. Phys Chem Mineral 10:27–37
Qin Z (1992) Disequilibrium partial melting model and its implications for trace element fractionations during mantle melting. Earth Planet Sci Lett 112:75–90
Ryerson FJ, McKeegan KD (1994) Determination of oxygen self-diffusion in akermanite, anorthite, diopside, and spinel: implications for oxygen isotopic anomalies and the thermal histories of Ca–Al-rich inclusions. Geochim Cosmochim Acta 58:3713–3734
Sammis CG, Smith JC, Schubert G (1981) A critical assessment of estimation methods for activation volume. J Geophys Res 86:10707–10718
Sautter V, Jaoul O, Abel F (1988) Aluminum diffusion in diopside using the $^{27}Al(p,\gamma)^{28}Si$ nuclear reaction: preliminary results. Earth Planet Sci Lett 89:109–114

Shannon RD (1976) Revised effective ionic radii and systematic studies of interatomic distances in halides and chalcogenides. Acta Cryst A32:751–767
Shimizu N (1981) Trace element incorporation into growing augite phenocryst. Nature 289:575–577
Simons B (1986) Temperatur- und Druckabhängigkeit der Fehlstellenkonzentration der Olivine und Magnesiowüstite. Habilitation Thesis, Univ Kiel, Germany
Smyth JR, Bish DL (1988) Crystal structures and cation sites of the rock forming minerals. Allen and Unwin, Boston
Sneeringer MA (1981) Strontium and samarium diffusion in diopside. PhD Thesis, Massachusetts Institute of Technology, Cambridge
Sneeringer M, Hart SR, Shimizu N (1984) Strontium and samarium diffusion in diopside. Geochim Cosmochim Acta 48:1589–1608
Ulmer P, Luth RW (1991) The graphite–COH fluid equilibrium in P, T, f_{O2} space: an experimental determination to 30 kbar and 1600 °C. Contrib Mineral Petrol 106:265–272
Van Orman JA (2000) Kinetics of chemical exchange during melting of planetary interiors. PhD Thesis, Massachusetts Institute of Technology, Cambridge
Van Orman JA, Grove TL (2000) Origin of high-titanium ultramafic glasses: constraints from phase relations and dissolution kinetics of clinopyroxene–ilmenite cumulates. Meteor Planet Sci 35:783–794
Van Orman JA, Grove TL, Shimizu N (1998) Uranium and thorium diffusion in diopside. Earth Planet Sci Lett 160: 505–519
Watson EB (1996) Surface enrichment and trace-element uptake during crystal growth. Geochim Cosmochim Acta 60: 5013–5020
Watson EB, Liang Y (1995) A simple model for sector zoning in slowly grown crystals: implications for growth rate and lattice diffusion, with emphasis on accessory minerals in crustal rocks. Am Mineral 80:1179–1187
Williams DW, Kennedy GC (1969) Melting curve of diopside to 50 kilobars. J Geophys Res 74:4359–4366
Zener C (1952) Theory of diffusion. In: Shockley W, Hollomon JH, Maurer R, Seitz F (eds) Imperfections in nearly perfect crystals. Wiley, New York, pp 289–314
Zindler A, Hart SR (1986) Chemical geodynamics. Annu Rev Earth Planet Sci 14:493–571